Journal of Magnetic Resonance 201 (2009) 218–221

Contents lists available at ScienceDirect

Journal of Magnetic Resonance

journal homepage: www.elsevier.com/locate/jmr

Dynamics of SARS-coronavirus HR2 domain in the prefusion and transition states

Susanna McReynolds [a], Shaokai Jiang [b], Lijun Rong [c], Michael Caffrey [a,*]

[a] Department of Biochemistry and Molecular Genetics, College of Medicine, University of Illinois at Chicago, Chicago, IL 60607, USA
[b] Research Core Facilities, University of Missouri, Columbia, MO 65211, USA
[c] Department of Microbiology and Immunology, College of Medicine, University of Illinois at Chicago, Chicago, IL 60612, USA

ARTICLE INFO

Article history:
Received 25 June 2009
Revised 15 September 2009
Available online 19 September 2009

Keywords:
Coronavirus
Dynamics
Heptad repeat
Membrane fusion
NMR
Relaxation
SARS-CoV

ABSTRACT

The envelope glycoproteins S1 and S2 of severe acute respiratory syndrome coronavirus (SARS-CoV) mediate viral entry by conformational change from a prefusion state to a postfusion state that enables fusion of the viral and target membranes. In this work we present the characterization of the dynamic properties of the SARS-CoV S2-HR2 domain (residues 1141–1193 of S) in the prefusion and newly discovered transition states by NMR ^{15}N relaxation studies. The dynamic properties of the different states, which are stabilized under different experimental conditions, extend the current model of viral membrane fusion and give insight into the design of structure-based antagonists of SARS-CoV in particular, as well as other enveloped viruses such as HIV.

SARS-CoV[1] (severe acute respiratory syndrome coronavirus) enters target cells by first binding to the cell membrane and subsequently inducing fusion of the viral and cellular membranes [1,2]. The envelope proteins S1 and S2 mediate the binding and fusion steps, respectively [3], in a manner that is thought to be similar to the well-characterized envelope proteins of HIV and influenza [4,5]. During the fusion step, SARS-CoV S2, as well as its homologs in HIV and influenza, is thought to undergo a series of conformational changes from a prefusion state to a postfusion state [1–5]. SARS-CoV S2 possesses 2 heptad repeat domains termed HR1 and HR2, which have a high propensity to form helix. The high-resolution structure of the SARS-CoV S2 in the postfusion state has been determined [6–8]. In the postfusion state of SARS-CoV S2, as well as the postfusion form of the analogous proteins in Ebola, HIV, influenza and parainfluenza [9–12], the HR1 domains self associate as parallel trimers and the HR2 domains associate with the HR1 in an anti-parallel orientation to form the "6 helix bundle". More recently structures of the prefusion states of SARS-CoV S2-HR1 [8] and S2-HR2 [13] have been determined. Other examples of prefusion structures include influenza HA2 [14] and parainfluenza virus 5 F [15]. Support for the presence of the prefusion conformation *in vivo* arises from the anti-viral activities of peptides, corresponding to the HR1 and HR2 sequences, that apparently inhibit virus entry by binding to the prefusion conformation and thereby prohibit the transformation to the postfusion form [16–18]. A peptide termed T20 or fuzeon, which stems from the HIV gp41 HR2 sequence, is currently used in humans [19].

A central feature of the viral entry model is the transformation from the prefusion state to the postfusion state. Recently, S2-HR2 has been shown to be in a dynamic equilibrium between a structured coiled-coil trimer, which is thought to represent the prefusion state, and unstructured monomer, which is thought to represent a metastable transition state [20]. In the present work, we present the detailed characterization of the dynamic properties of SARS-CoV S2-HR2 in the prefusion and transition states using NMR relaxation. We will discuss the importance of considering the S2-HR2 dynamic properties in the viral entry model, as well as in the design of future envelope-based anti-virals.

Recombinant SARS-CoV S2-HR2, consisting of residues 1141–1193 of S, was prepared as previously described [13]. NMR samples were prepared by ultrafiltration (YM3, Amicon, Billerica, MA) using the appropriate buffer (10 mM PO_4/pH 7.0 or 10 mM PO_4/pH 7.0, 30% TFE-*d3*, Cambridge Isotope Laboratories, Andover, MA). The final concentration of S2-HR2 was 400 μM (R_{xy} of the prefusion state was also determined at 1 mM protein concentration). NMR spectra were recorded on a Bruker AVANCE 800 MHz spectrometer equipped with a cryogenic triple resonance probe. Spectra were processed by NmrPipe and visualized with NmrDraw [21]. The backbone assignments at 25 °C in the presence and absence of 30% TFE have been reported elsewhere [13,20]. The backbone assignments of S2-HR2 at 45 °C were determined from a series of the standard triple resonance experiments [13]. The ^{15}N $R_z(1/T_1)$,

* Corresponding author. Address: Department of Biochemistry and Molecular Genetics, College of Medicine, University of Illinois at Chicago, MC669, 900 S. Ashland Ave., Chicago, IL 60607, USA. Fax: +1 312 413 0364.

[1] *Abbreviations:* CoV, coronavirus; HR, heptad repeat; SARS, severe acute respiratory syndrome; TFE, trifluoroethanol.

1090-7807/$ - see front matter © 2009 Elsevier Inc. All rights reserved.
doi:10.1016/j.jmr.2009.09.012

$R_{xy}(1/T_2)$ and HNOE values were measured by standard pulse sequences [22]. For determination of R_z, the delay values were set to: 30, 60, 120, 240, 72 and 1250 ms (prefusion state); 50, 100, 200, 400, 800 and 1200 ms (transition state). For determination of R_{xy}, the delay values were set to: 8, 16, 32, 64, 96, 128, 256 and 512 ms (prefusion state); 10, 20, 40, 80, 128 and 256 ms (transition state). The decays of cross-peak intensities with time in the ^{15}N R_z and R_{xy} experiments were fit to a single exponential by a non-linear least-squares fit with fitting errors typically less than 5% (Kaleidagraph 3.08, Synergy Software). No significant difference for the prefusion R_{xy} was observed for two different concentrations, 400 μM and 1 mM, suggesting that R_{xy} was not dependent on concentration. HNOE values for each given residue were calculated as the intensity ratio (I/I_0) of the ^{15}N–^{1}H correlation peak in the presence (I) and absence (I_0) of proton saturation during the relaxation delay of 5 s. Errors in the HNOE were estimated to be ±0.10 from the S/N ratios. For reduced spectral density mapping, the spectral density functions were described as:

$$J(0) = (6R_{xy} - 3R_z - 2.72\sigma_{NH})/(3d^2 + 4c^2)$$

$$J(\omega_N) = (4R_z - 5\sigma_{NH})/(3d^2 + 4c^2)$$

$$J(0.87\omega_H) = 4\sigma_{NH}/(5d^2)$$

where $\sigma_{NH} = R_z(\mathrm{NOE} - 1)\gamma_N/\gamma_H$; $d = (\mu_0 h\gamma_N\gamma_H)/(8\pi^2 r^3)$; $c = \omega_N\Delta\sigma/3^{1/2}$; γ_N and γ_H are the gyromagnetic ratios of ^{15}N and ^{1}H, respectively; μ_0 is the free space permeability; h is Planck's constant divided by 2π; r is the length of the ^{1}H–^{15}N bond, 1.04 Å; ω_N and ω_H are the Larmor frequencies of ^{15}N and ^{1}H, respectively; $\Delta\sigma$ is the ^{15}N CSA of −162 ppm [23]. Errors of the spectral density functions were determined by propagating the uncertainties of the individual relaxation parameters.

S2-HR2 exists in different conformational states, which are dependent upon the experimental conditions. For example, at 25 °C in the presence of 30% TFE, S2-HR2 is a stable coiled-coil trimer, which represents the prefusion state [13]. On the other hand, in the absence of co-solvent, at 25 °C S2-HR2 is in equilibrium between unstructured monomer and a structured trimer, which is thought to represent an equilibrium between the prefusion and transition states [20]. Moreover, in the absence of co-solvent, S2-HR2 exhibits a melting temperature of ~35 °C and is completely unstructured at 45 °C [20]. To gain insight into the dynamic properties of the prefusion and transition states, we characterized the dynamic properties of S2-HR2 under two experimental conditions: 10 mM $NaPO_4$/pH 7.0, 30% TFE at 25 °C (prefusion state) and 10 mM $NaPO_4$/pH 7.0 at 45 °C (transition state). NMR relaxation is correlated to the global correlation time τ_c, which can be estimated from the Stokes equation ($\tau_c = (4\pi r^3\eta)/(3k_bT)$, where r = radius, η = viscosity, k_b = Boltzman's constant and T = temperature). Consequently, the interpretation of the NMR relaxation properties of S2-HR2 must take into consideration the temperature, solvent viscosity, and protein molecular volume, of S2-HR2 as summarized in Table 1. For example, the estimated τ_c of the transition state (i.e. unstructured monomer) is predicted to be a factor of ~4 less than that of the prefusion state (i.e. structured trimer in the presence of co-solvent).

The dynamic properties of S2-HR2 under two different experimental conditions were characterized by determination of heteronuclear relaxation rates of the NH, which have been widely used to investigate the backbone dynamics of proteins and the role of dynamics in protein function [26,27]. The ^{15}N R_z and R_{xy} relaxation rates and the ^{1}H–^{15}N NOE (HNOE) at 800 MHz of S2-HR2 are shown in Fig. 1 (cf. Supplementary Tables 1 and 2). The average R_z, R_{xy} and the HNOE values of the prefusion S2-HR2 helix (residues 17–47 of the construct, residues 1155–1185 of S) are summarized in Table 2. The values for the prefusion state suggest a helix exhibiting a relatively rigid region with increased flexibility at its C-terminal end, and flexible N- and C-terminal regions. The relaxation values for the transition state are consistent with the faster molecular tumbling of a smaller molecule under conditions of higher temperature and lower solvent viscosity (Table 1). The relative uniformity and magnitude of the transition state relaxation parameters for residues 17–47 support the notion that under these conditions S2-HR2 is monomeric with little residual structure present. Nonetheless, the termini of the transition state are clearly more flexible on the ps–ns timescale as indicated by the negative HNOE.

Table 1
Predicted molecular dynamic properties of SARS-CoV S2-HR2 (residues 1–55 of the construct, residues of 1141–1193 of S).

State[a]	T (°C)	M_W (kDa)	η (cP)	τ_c/τ_{cref}[b]
Transition	45	6.3[c]	0.61	0.23
Prefusion	25	18.6[d]	1.63	1.00

[a] Transition = 10 mM $NaPO_4$/pH 7.0 at 45 °C; prefusion = 10 mM $NaPO_4$/pH 7.0, 30% TFE at 25 °C.
[b] ($\tau_c = (4\pi r^3\eta)/(3k_bT)$, where r = radius, η = viscosity, k_b = Boltzman's constant and T = temperature) and $\tau_{cref} = \tau_c$ of the structured trimer (i.e. at 10 mM $NaPO_4$/pH 7.0, 30% TFE at 25 °C). $R_{monomer}$ is taken to be 23.1 Å, which is based on the experimental value for protein G, a protein with an identical number of residues, under denaturing conditions [24]. R_{trimer} is taken to be 26.7 Å, as calculated by CNS [25] using the coordinates for the prefusion form [13].
[c] Based on monomer–trimer equilibrium in fast exchange at 25 °C (70% monomer/30% trimer) and the lack of structure at 45 °C (100% monomer) [20].
[d] Based on the solution structure and analytical centrifugation studies [13].

The reduced spectral density functions $J(0)$, $J(\omega_N)$ and $J(0.87\omega_H)$ are correlated with the magnitude of NH bond fluctuations at three different frequencies. In contrast to the widely used model free formalism, spectral density functions make no assumptions for a motional model with a uniform τ_c and thus spectral density functions are clearly most appropriate for the analysis of the dynamic properties of partially unfolded and unstructured regions [23], which is clearly relevant in the case of S2-HR2. In Fig. 2, the $J(0)$, $J(\omega_N)$ and $J(0.87\omega_H)$ values are shown for the residues of S2-HR2 under the two experimental conditions. The average spectral density values of the prefusion S2-HR2 helix (residues 17–47 of the construct, residues 1155–1185 of S) are summarized in Table 2. In the prefusion state, higher $J(0)$ values are found in the helix and lower $J(0)$ are found at the termini, which is consistent with the presence of a coiled-coil core on the ns timescale. In the case of the transition state, lower and more uniform $J(0)$ are exhibited, consistent with an unstructured monomer. The uniform dynamic profile of the S2-HR2 transition state resembles that of the urea-denatured protein G [28]. Note that the ratio of the $J(0)$ values can be used to estimate the ratio of the τ_c values. For example, the ratio of the helix region of the transition state $J(0)$ to that of the prefusion $J(0)$ is 0.24, which is in very good agreement with that predicted in Table 1 (the prefusion state τ_c is predicted to be ~4× that of the transition state τ_c), especially considering the difficulty in estimating the molecular volume of the unstructured monomer. With respect to the high frequency motions reflected by $J(\omega_N)$ and $J(0.87\omega_N)$, the prefusion state exhibits significantly lower ps motions in the helix with respect to the transition state. However, the C-terminal region of the prefusion helix, consisting of ~8 residues, exhibit increased dynamic motions similar to that observed for $J(0)$. Interestingly, this region is not helical in the absence of co-solvent [20] and thus the increased dynamics may be reporting a region of inherent instability. In contrast, NMR dynamic studies have generally shown that helices exhibit uniform fast time scale dynamics with small increases in ns–ps motions at the terminal three residues of the helix [29]. A notable exception has been observed for the basic leucine zipper of GCN4, which is another coiled-coil helix [30].

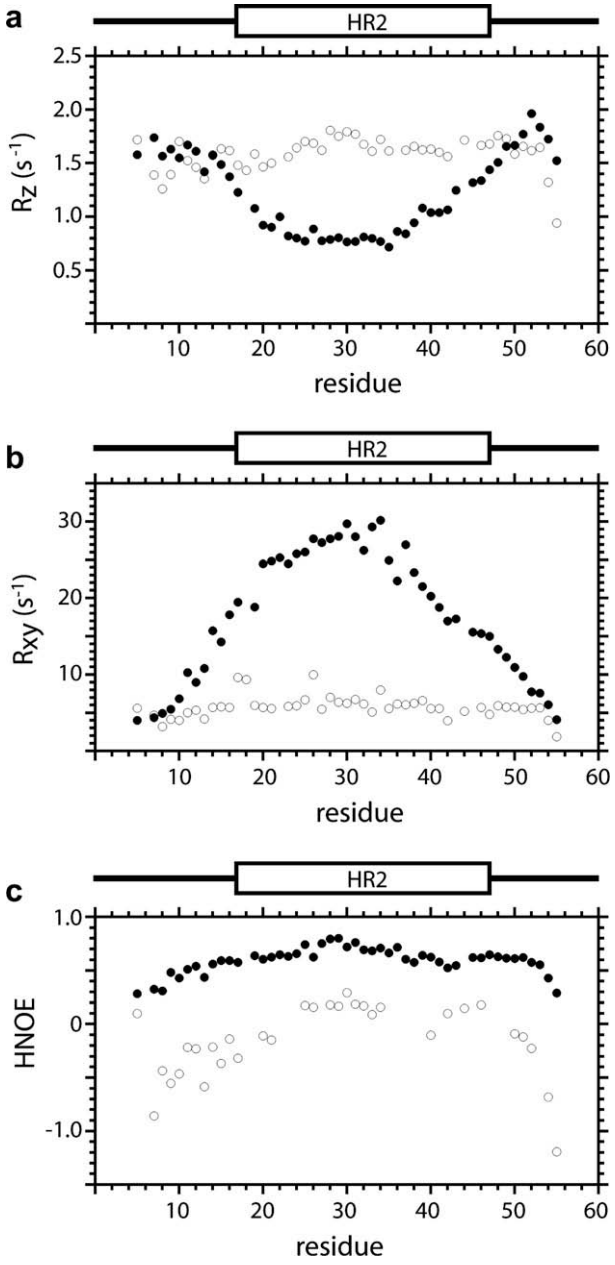

Fig. 1. ^{15}N relaxation parameters of SARS-CoV S2-HR2 under two different experimental conditions: (a) ^{15}N R_z, (b) ^{15}N R_{xy} and (c) HNOE. Experimental conditions were 400 μM S2-HR2 in 10 mM PO_4/pH 7.0, 30% TFE at 25 °C (filled circles) and 400 μM S2-HR2 in 10 mM PO_4/pH 7.0 at 45 °C (open circles).

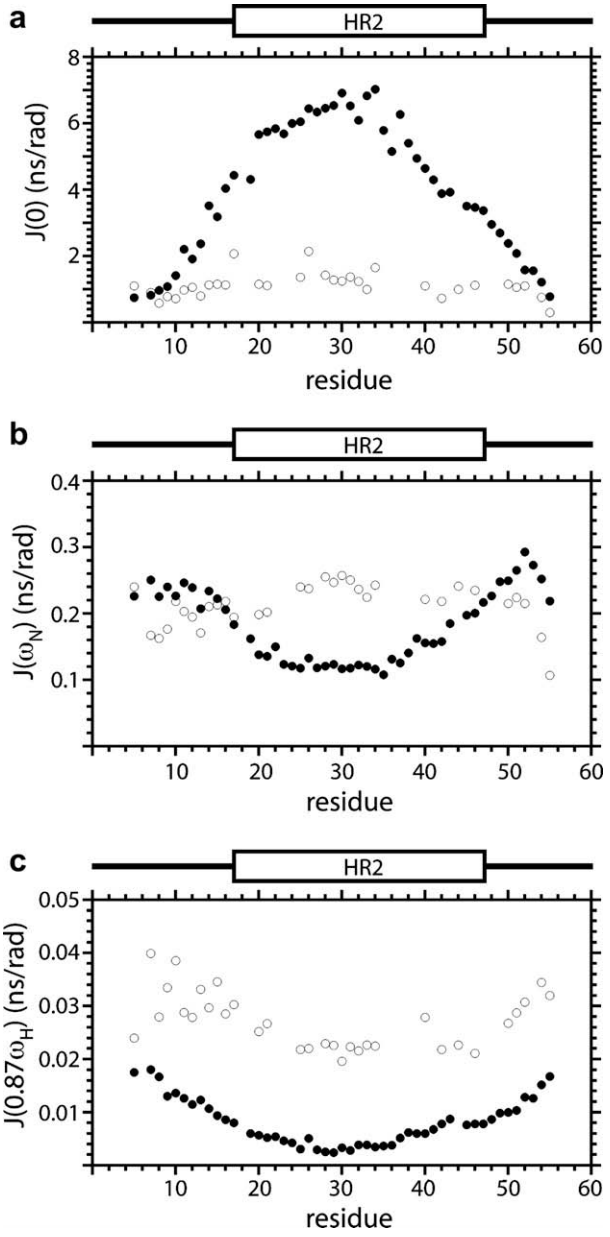

Fig. 2. Reduced spectral density mapping of SARS-CoV S2-HR2 under two different experimental conditions: (a) $J(0)$, (b) $J(\omega_N)$ and (c) $J(0.87\omega_H)$. Experimental conditions were 400 μM S2-HR2 in 10 mM PO_4/pH 7.0, 30% TFE at 25 °C (filled circles) and 400 μM S2-HR2 in 10 mM PO_4/pH 7.0 at 45 °C (open circles).

Table 2
Average relaxation parameters in the SARS-CoV S2-HR2 helix (residues 17–47 of the construct, residues 1155–1185 of S).

Relaxation parameter	Prefusion[a]	Transition[b]
R_z (s^{-1})	0.95 ± 0.20	1.64 ± 0.10
R_{xy} (s^{-1})	23.5 ± 4.7	6.33 ± 1.39
HNOE	0.66 ± 0.07	0.08 ± 0.16
$J(0)$ (ns/rad)	5.44 ± 1.12	1.32 ± 0.37
$J(\omega_N)$ (ns/rad)	0.14 ± 0.03	0.23 ± 0.02
$J(0.87\omega_H)$ (ns/rad)	0.0052 ± 0.0019	0.023 ± 0.003

[a] Experimental conditions were 400 μM S2-HR2 in 10 mM $NaPO_4$/pH 7.0, 30% TFE at 25 °C.
[b] Experimental conditions were 400 μM S2-HR2 in 10 mM $NaPO_4$/pH 7.0 at 45 °C.

In summary, the relaxation properties of S2-HR2 are consistent with the model of an equilibrium between a prefusion state with a coiled-coil trimer conformation and a transition state comprised of unstructured monomer [20]. In Fig. 3, such a model is presented with the structural and dynamic properties of the two states summarized. An important feature of this model is that the transition state enables the conformational changes of envelope necessary for SARS-CoV entry (i.e. interaction between HR2 and HR1 to form the 6 helix bundle). Based on the present characterization of the S2-HR2 dynamic properties, the transition state may accomplish this by efficient sampling of a large area of conformational space. Finally, we note that, due to the very different structural and dynamic properties of the prefusion and transition states, consideration of the their structural and dynamic properties may be of importance in the design of HR2-based anti-virals for SARS-CoV

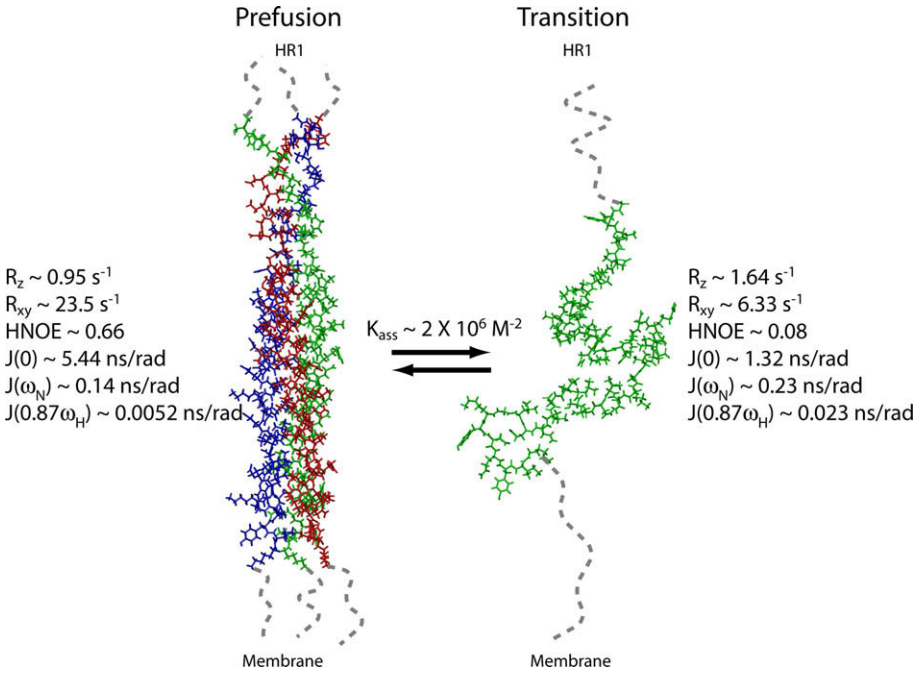

Fig. 3. Model of SARS-CoV S2-HR2 prefusion and transition states. The average relaxation parameters shown are those for the prefusion helix (residues 17–47 of the construct, residues 1155–1185 of S) and the analogous region of the transition state. Note that the prefusion and transition state values were acquired at different temperatures and solvent viscosities (cf. Table 1). The relative locations of the HR1 and transmembrane domains, which occur at the N- and C-termini of S2-HR2, respectively, are depicted by dotted lines. The structure of the prefusion state is taken from Hakansson-McReynolds et al. [13] with each subunit colored differently; the structure of the transition state was modeled by torsion angle simulated annealing of the S2-HR2 monomer in the absence of NMR restraints. The equilibrium constant shown was estimated from the observation that the ^{13}C secondary chemical shifts of the S2-HR2 helix at 25 °C are ~30% of the magnitude observed in the presence of TFE [20].

in particular and perhaps analogous HR2-based anti-virals for other viruses such as HIV.

Acknowledgment

This work was partially supported by grants from the NSF and NIH.

Appendix A. Supplementary data

Two tables containing the relaxation data (R_z, R_{xy} and HNOE) and the reduced spectral density values ($J(0)$, $J(\omega_N)$ and $J(0.87\omega_H)$) for SARS-CoV S2-HR2 under different experimental conditions. Supplementary data associated with this article can be found, in the online version, at doi:10.1016/j.jmr.2009.09.012.

References

[1] G. Simmons, J. Reeves, A. Rennekamp, S. Amberg, A. Piefer, P. Bates, Proc. Natl. Acad. Sci. USA 101 (2004) 4240–4245.
[2] H. Hofmann, S. Pohlmann, Trends Microbiol. 12 (2004) 466–472.
[3] T. Gallagher, M. Buchmeier, Virology 279 (2001) 371–374.
[4] D.M. Eckert, P.S. Kim, Annu. Rev. Biochem. 70 (2001) 777–810.
[5] S. Gallo, C. Finnegan, M. Viard, Y. Raviv, A. Dimitrov, S. Rawat, A. Puri, S. Durrell, R. Blumenthal, Biochim. Biophys. Acta 1614 (2003) 36–50.
[6] Y. Xu, Z. Lou, Y. Liu, H. Pang, P. Tien, G. Gao, Z. Rao, J. Biol. Chem. 279 (2004) 49414–49419.
[7] V. Supekar, C. Bruckmann, P. Ingallinella, E. Bianchi, A. Pessi, A. Carfi, Proc. Natl. Acad. Sci. USA 101 (2004) 17958–17963.
[8] Y. Deng, J. Liu, Q. Zheng, W. Yong, M. Lu, Structure 14 (2006) 889–899.
[9] W. Weissenhorn, A. Carfi, K.H. Lee, J.J. Skehel, D.C. Wiley, Mol. Cell 2 (1998) 605–616.
[10] M. Caffrey, M. Cai, J. Kaufman, S.J. Stahl, P.T. Wingfield, A.M. Gronenborn, G.M. Clore, EMBO J. 17 (1998) 4572–4584.
[11] P. Bullough, F. Hughson, J. Skehel, D. Wiley, Nature 371 (1994) 37–43.
[12] H.S. Yin, R.G. Paterson, X. Wen, R.A. Lamb, T.S. Jardetzky, Proc. Natl. Acad. Sci. USA 102 (2005) 9288–9293.
[13] S. Hakansson-McReynolds, S. Jiang, L. Rong, M. Caffrey, J. Biol. Chem. 281 (2006) 11965–11971.
[14] I.A. Wilson, J.J. Skehel, D.C. Wiley, Nature 289 (1981) 366–373.
[15] H. Yin, X. Wen, R. Paterson, R. Lamb, T. Jardetzky, Nature 439 (2006) 38–44.
[16] C. Wild, D. Shugars, T. Greenwell, C. McDanal, T. Matthews, Proc. Natl. Acad. Sci. USA 91 (1994) 9770–9774.
[17] B. Bosch, B. Martina, R. Van Der Zee, J. Lepault, B. Haijema, C. Versluis, A. Heck, R. De Groot, A. Osterhaus, P. Rottier, Proc. Natl. Acad. Sci. USA 101 (2004) 8455–8460.
[18] S. Liu, G. Xiao, Y. Chen, Y. He, J. Niu, C. Escalente, H. Xiong, J. Farmar, A. Debnath, P. Tien, S. Jiang, Lancet 363 (2004) 938–947.
[19] J. Kilby, J. Lalezari, J. Eron, M. Carlson, C. Cohen, R. Arduino, J. Goodgame, J. Gallant, P. Volberding, R. Murphy, F. Valentine, M. Saag, E. Nelson, P. Sista, A. Dusek, AIDS Res. Hum. Retroviruses 1 (2002) 685–693.
[20] S. McReynolds, S. Jiang, G. Ying, J. Celigoy, C. Schar, L. Rong, M. Caffrey, Biochemistry 47 (2008) 6802–6808.
[21] F. Delaglio, S. Grzesiek, G.W. Vuister, G. Zhu, J. Pfeifer, A. Bax, J. Biomol. NMR 6 (1995) 277–293.
[22] S. Hakansson, M. Caffrey, Biochemistry 42 (2003) 8999–9006.
[23] W. Farrow, O. Zhang, A. Szabo, D. Torchia, L. Kay, J. Biomol. NMR 6 (1995) 153–162.
[24] N. Fitzkee, G. Rose, Proc. Natl. Acad. Sci. USA 101 (2004) 12497–12502.
[25] A. Brunger, P. Adams, G. Clore, W. DeLano, P. Gros, R. Grosse-Kunstleve, J.-S. Jiang, J. Kuszewski, M. Nilges, N. Pannu, R. Read, L. Rice, T. Simonson, G. Warren, Acta Crystallogr. D54 (1998) 905–921.
[26] A. Palmer, Annu. Rev. Biophys. Biomol. Struct. 30 (2001) 129–155.
[27] V. Jarymowcyz, M. Stone, Chem. Rev. 106 (2006) 1624–1671.
[28] M. Frank, G. Clore, A. Gronenborn, Protein Sci. 4 (1995) 2605–2615.
[29] J. Goodman, M. Pagel, M. Stone, J. Mol. Biol. 295 (2000) 963–978.
[30] C. Bracken, P. Carr, J. Cavanagh, A. Palmer, J. Mol. Biol. 285 (1999) 2133–2146.